Available online at www.sciencedirect.com
ScienceDirect
Polymer 48 (2007) 5161–5173
polymer
www.elsevier.com/locate/polymer

Molecular structure of side-chain liquid crystalline polysiloxane in the smectic C phase from X-ray diffraction and molecular modeling

Kuei-Jen Lee [a,*], Ging-Ho Hsiue [b], Jung-Lung Wu [b], Yi-An Sha [b]

[a] Department of Bioinformatics, Asia University, Taichung 413, Taiwan, ROC
[b] Department of Chemical Engineering, National Tsing Hua University, Hsinchu 300, Taiwan, ROC

Received 25 September 2006; received in revised form 20 June 2007; accepted 21 June 2007
Available online 27 June 2007

Abstract

The structure of a side-chain liquid crystalline polysiloxane containing two oligo(oxyethylene) units and (*R*)-1-methylheptyl 4-(4-hydroxybiphenyl-4′-carbonyloxy) benzoate mesogens (PS221B) has been studied using X-ray diffraction patterns and molecular modeling. Ten periodic simulated cells with equilibrated structures are generated, each containing 35 mesogenic groups and a polysiloxane backbone. The simulated X-ray diffraction patterns are in agreement with those obtained experimentally. The calculated width of the sublayers of the polysiloxane backbone is about 5.63 Å along the *z*-axis. The distributions of the dihedral angles of the polysiloxane backbone in the equilibrated structures indicate that the backbone has a higher probability distribution in the *trans* state. The distributions of the dihedral angles at the bonds in the aromatic core of the mesogenic groups reveal high probabilities of the *trans* and *cis* placements. The local order due to the interactions between the aromatic cores is in the range of 3–5 Å. The order of the radial distribution function vanishes beyond this range.

Keywords: Side-chain liquid crystalline polymer; X-ray diffraction; Molecular modeling

1. Introduction

Smectic liquid crystals [1,2], formed either by monomeric liquid crystals or by side-chain liquid crystalline polymers, have revealed as a variety of layered phases, and characterized by both the orientational and translational orders. Among various layered phases, the smectic C (Sc) phase has attracted much interest due to its unique molecular assembly and electro-optical applications [3]. Hsiue et al. have studied not only low molar mass smectic liquid crystals [4–6] but also side-chain liquid crystalline polymers [7–10]. The mesogenic groups are composed of oligo(oxyethylene) spacers, various chiral moieties, and two or three aromatic rings of ester core units, of which many exhibited a broad temperature range of chiral smectic C (S_{C^*}) phase and satisfactory electro-optical properties. For this work, we have studied a new series of side-chain liquid crystalline polysiloxanes, whose mesogenic pendants correspond to a series of compounds in our previous work [6]. Thus, the side chains containing 0–3 oligo(oxyethylene) units, a phenyl biphenyl carboxylate mesogenic group, and an (*R*)-1-methylheptyloxycarbonyl tail have been synthesized. These synthesized polymers are abbreviated as PS*n*21B (Fig. 1). The developed polymers are characterized by differential scanning calorimetry (DSC), optical polarizing microscopy, and high resolution X-ray diffraction measurements. Furthermore, one of the polymers, PS221B ($n = 2$), is investigated using atomistic modeling, to study the bulk properties and molecular structures.

The molecular structures of the mesogens of side-chain liquid crystalline polymers are important since the structures determine the interactions between the mesogens and their relative orientations. The molecular assembly of a smectic mesophase is based on the interactions within each smectic layer, and as well the interactions play an essential role in various kinds of liquid crystalline phase transitions. The *d*-spacings obtained from the X-ray results [11,12] of smectic liquid crystals inferred that mesogens form a model which can be completely

* Corresponding author. Tel.: +886 4 2339 8316; fax: +886 4 2332 0718.
E-mail address: kjlee@asia.edu.tw (K.-J. Lee).

0032-3861/$ - see front matter © 2007 Elsevier Ltd. All rights reserved.
doi:10.1016/j.polymer.2007.06.045

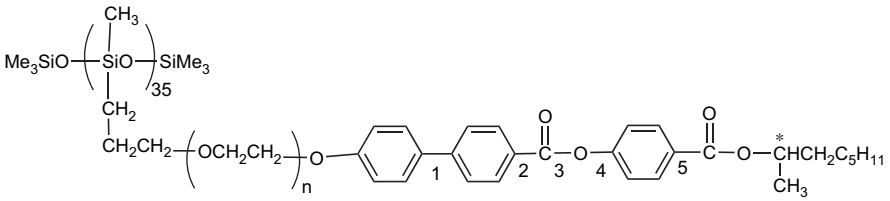

Fig. 1. Chemical/structural formula for PS*n*21B. The indices 1–5 at the bonds in the aromatic core are labeled for the calculations of dihedral angles.

interdigitated, partially interdigitated, or non-interdigitated with their neighbors. The interdigitated structures of monomeric liquid crystals have been investigated using dimer associations. Based on intermolecular interactions of two monomeric molecules, two possible configurations are available: parallel and antiparallel alignments. Molecular modeling [13–16] and theoretical approaches [17–19] have addressed this problem to more thoroughly understand the dimer associations. In our previous work, a series of ferroelectric liquid crystals with low molar mass, namely MD*n*21B [6], has been synthesized and characterized, as well as investigated using atom-based molecular modeling [16] and molecular dynamics simulations [20]. According to our computer simulations [16], the dimers composed of MD221B molecules display the configuration with completely antiparallel association, and end-to-end distances of the dimers are nearly consistent with the *d*-spacings of the smetic layers of PS221B. Therefore, we can infer that PS221B belongs to a completely interdigitated structure.

In side-chain liquid crystalline polymers, the flexible polymer backbones and spacers allow the attached mesogens to form their favorable packing structures. Thus, the structures of the polymer backbones may also play an important role in liquid crystalline phase formation. The backbone configuration of side-chain liquid crystalline polymers has been extensively studied using small-angle neutron scattering (SANS) [21–24] or X-ray diffraction experiments [25,26]. As shown in the results of Noirez et al. [22], the configuration of the backbone for polyacrylates, polymethacrylates, or poly(methylsiloxane) in the smectic phases is oblate, and the shape depends on temperature conditions. The oblate shape demonstrates that the polymer backbones are confined between the liquid crystal layers. The overall configuration of the liquid crystalline polymers is considered, where the averaged direction of a backbone is perpendicular to the liquid crystalline director **n**. X-ray diffraction studies [25] of the backbone of side-chain poly(methylsiloxanes) display the electron density profiles, which indicate that polysiloxanes are confined between sublayers with the widths ranging between 5 and 7 Å along the director **n**, which are comparable to the results of small-angle neutron scattering experiments [22] for the backbone of polymethacrylates. Also the results indicate that the polymer backbones are squeezed by liquid crystal layers and show that the backbones have a quasi-bidimensional configuration, similar to that of polymer chains confined between hard walls [27–29].

The investigations of the structure and property relationships in liquid crystalline materials at the molecular level are important because the electro-optical properties are influenced by molecular structures of the liquid crystals. Recently, molecular modeling plays an important role in revealing the bulk structures of the desired compounds on a molecular level, which sometimes proves difficult to achieve in experimental studies. Therefore, molecular modeling is a good technique to complement experimental results used to characterize the structures and properties of liquid crystalline materials. Molecular modeling has been well established in the simulations of low molecular weight liquid crystals [30]. However, some progress has been made in the modeling of side-chain liquid crystalline polymers [31–34] and of main chain liquid crystalline polymers [35–39] either by molecular mechanics or by molecular dynamics simulations.

Hence, we are motivated to study a new compound PS221B using atom-based molecular modeling. Among PS*n*21B polymers, we are particularly interested in PS221B compound, since it exhibits a wide temperature range of S_{C^*} phase (around 130 °C) and shows simple phase transitions (Fig. 2).

In this study, 10 simulated models of PS221B are generated using molecular dynamics, so that we can study the bulk properties of PS221B on this ensemble. Simulations are performed on equilibrated models to obtain simulated X-ray diffraction

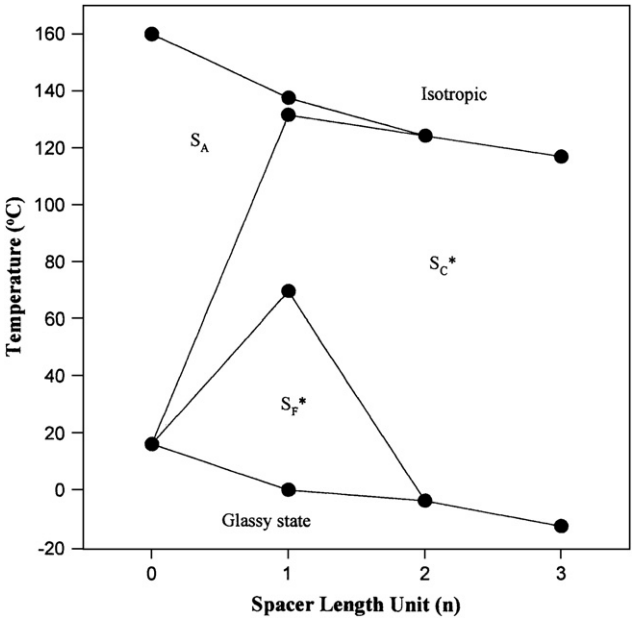

Fig. 2. Plot of transition temperatures versus *n*, the number of oxyethylene spacer units, for PS*n*21B.

patterns, the *d*-spacings of smectic layers, the orientations of mesogenic groups, and the distributions of dihedral angles, in polysiloxane backbone and in aromatic core of mesogenic groups, as well as the configurations of the polysiloxane backbone confined between the liquid crystalline layers. The distributions of dihedral angles and the bond direction correlation function of the backbone in the equilibrated models are compared to those of an isolated poly(dimethylsiloxane) (PDMS) chain, generated with 10 random structures in vacuum.

2. Experimental

In this study, the side-chain liquid crystalline polymers (PS*n*21B), as shown in Fig. 1, were prepared from MD*n*21B [6] and commercially available poly(methylhydrosiloxane) with an averaged degree of polymerization of 35. The detailed synthesis of these polymers was shown elsewhere [40]. In a DSC measurement (data not shown), the cooling scan shows an isotropic state to an S_{C*} transition and an S_{C*} to a glass transition temperature (T_g) at 124.2 °C and −3.2 °C, respectively. Fig. 2 displays the transition temperature of PS*n*21B as a function of *n*, the number of oxyethylene units, and reveals that all of the polymers have liquid crystalline mesomorphism. Therefore, the only mesophase that can be found for PS221B is the S_{C*} phase. In addition to DSC, X-ray diffraction measurements were also conducted to confirm the mesophases for these polymers. X-ray diffraction measurements were taken with a Rigaku R-Axis IIC powder diffractometer. Two imaging plate (abbreviated IP) detectors were used so that reflection spot exposure and readout operations could be performed. This feature provides efficient data collection and minimizes the time required for IP residual image erasure. The monochromatized X-ray beam from nickel-filtered Cu Kα radiation with a wavelength of 0.15406 nm was used. The resolution was 0.05° for scanning direction. Finally, a temperature controller was added to the X-ray apparatus for thermal measurements. The precision of the controller was ±0.5 °C in the temperature range studied. The X-ray diffraction patterns for PS221B show a decrease in the *d*-spacings of the first-order reflection from 32.35 Å to 32.03 Å as the measuring temperature decreased from 100 °C to 70 °C (Fig. 3). The results of optical polarizing microscopy show that the broken focal-conic textures can be observed in the S_{C*} phase for PS221B at 116.4 °C. The measured density for PS221B at room temperature was 1.13 g/cm^3.

3. Simulations

Simulations were performed for a side-chain liquid crystalline poly(methylsiloxane) (PS221B), as shown in Fig. 1. Ten simulated models of PS221B were generated and each model, based on the chemical structure given in Fig. 1, was generated into a periodic boundary cell. In a simulated model, 35 mesogenic groups were attached to a polysiloxane backbone having a degree of polymerization of 35. These mesogenic groups were originally from 4-(*R*)-1-methylheptyl [[[[4-(2-(2-(allyloxy)ethoxy)ethoxy)] biphenyl-4′-yl]carbonyl]oxy]benzoate

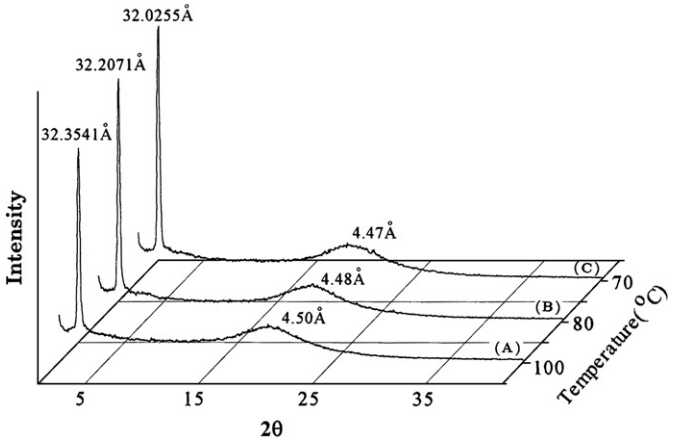

Fig. 3. Temperature dependence of powder X-ray diffraction measurements for polymer PS221B at (a) 100 °C, (b) 80 °C, and (c) 70 °C.

(MD221B) [6]. To understand thoroughly the difference between the structures of a backbone confined between liquid crystal layers and the structures of an isolated chain, an isolated PDMS chain with a degree of polymerization of 35 was also simulated for comparison. Thus, 10 initial configurations of this PDMS chain were generated independently with their dihedral angles assigned randomly.

According to the results of previous investigations [25,27,28], we could infer that the configurations of the polymer backbones of liquid crystalline polymers were similar to those of polymer chains confined between planar solid surfaces [27,28]. Therefore, the configuration of a backbone was initially obtained from an isotropic PDMS chain with a degree of polymerization of 35, which was compressed by two diamond surfaces, separated by a distance of 12 Å, along the *z*-axis. Fig. 4a shows that this PDMS chain confined by the two surfaces was relaxed by applying several cycles of energy

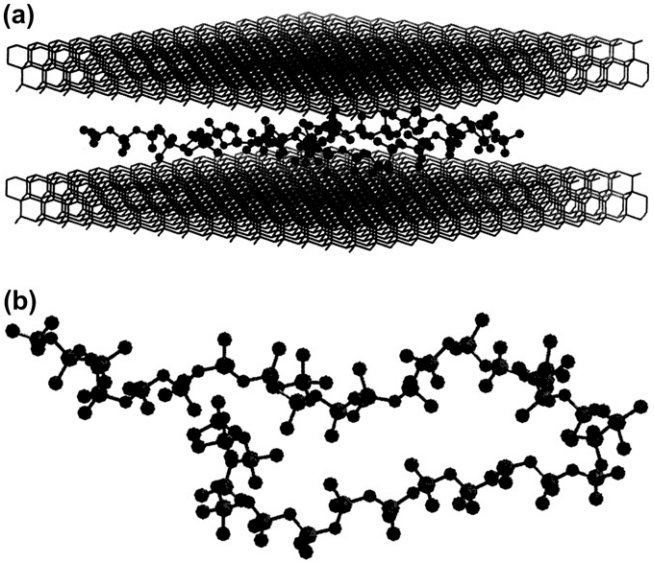

Fig. 4. (a) The assembly of diamond surfaces and a PDMS chain with a repeat unit of 35. (b) A quasi-bidimensional configuration of the PDMS chain. Hydrogen atoms are omitted in both (a) and (b).

minimization and molecular dynamics at 500 K. Fig. 4b displays an anisotropic configuration of this PDMS chain, as shown by a quasi-bidimensional random coil. When such a configuration was generated for a backbone, one of the two methyl groups at each silicon atom in the backbone was replaced by a mesogenic group as a side chain. From our previous work [16], the liquid crystalline monomers (MD221B) in a model of simulated smectic C phase were selected for this work as mesogenic groups, so that some modifications were made in the model to fit the simulations of a side-chain liquid crystalline polymer in the smectic C phase. For example, the antiparallel monomers in a simulated cell [16] were moved upwards or downwards along the z-axis of the simulated cell. The monomers were in a bilayer configuration, where the double-bonded end of each monomer was oriented towards the center of the bilayer. The already constructed backbone was moved to a position located between the double-bonded ends. Fig. 5 displays the mesogenic groups with the backbone having a quasi-bidimensional configuration in a periodic cell. These double bonds in the mesogenic groups

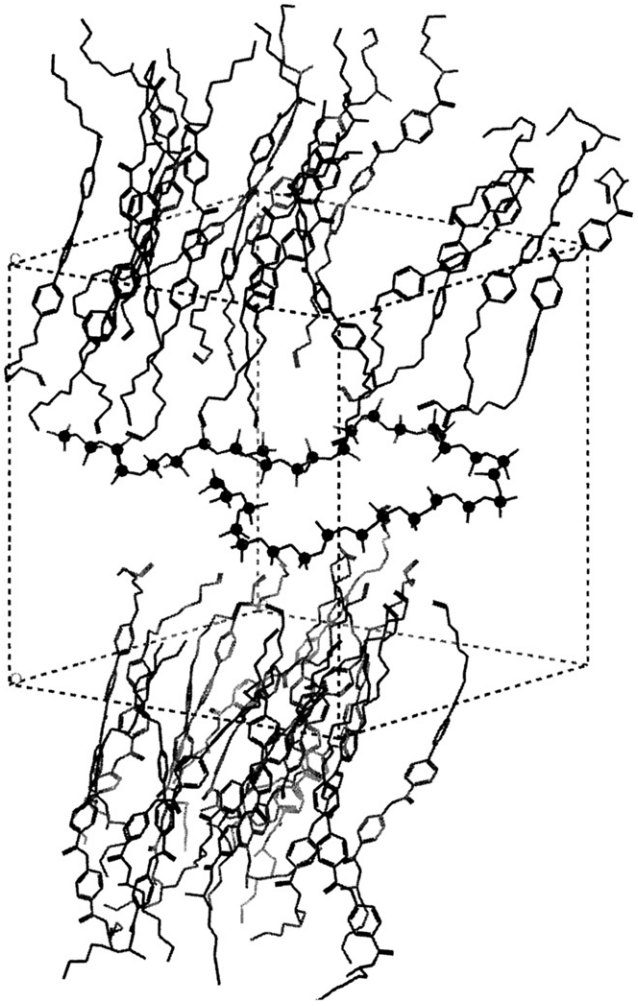

Fig. 5. Mesogenic groups and a PDMS chain acting as a backbone shown in a periodic simulation cell. The backbone is shown by a stick–ball representation, and hydrogen atoms are not shown.

were then connected with the backbone. Thus, an initial model of a side-chain liquid crystalline polysiloxane (PS221B) was constructed in a periodic boundary cell. The constructed initial model containing 3212 discrete atoms with hydrogen atoms explicitly included was used to generate 10 different structures by using a molecular dynamics run. The initial model was energy minimized using 500 steps of steepest descents to eliminate bad atomic contacts and then a molecular dynamics run was performed at 500 K for 100 ps. Ten conformations (structures) with relatively low total potential energy were saved during the molecular dynamics duration to represent the ensemble of the side-chain liquid crystalline polysiloxane (PS221B). These 10 saved structures were relaxed using a procedure similar to that used in previous investigations [41–44].

The saved structures were first minimized using steepest descents for 500 steps with cell parameters optimized. To prevent the saved structures from becoming trapped in a high energy state, molecular dynamics runs at a temperature of 500 K were performed after the initial energy minimization. The molecular dynamics was used to provide the kinetic energy required for conformational motions so that the structures could move out of the local energy minima. Cycles of energy minimization and molecular dynamics were then performed on the first minimized models with periodic boundary conditions, where the minimization method was changed to conjugate-gradients with the cell dimensions optimized. The molecular dynamics was conducted under a canonical (NVT) ensemble according to the Nosé thermal coupling method [45–47]. For the NVT ensemble, the number of atoms N, volume V, and the temperature T of the system were kept constant. The energy calculations were made according to the Dreiding II force field [48], as provided in Cerius^2 supplied by Accelrys, Inc. [49]. The total potential energy of the system, E_t, was calculated from the following terms:

$$E_t = E_l + E_\theta + E_\varphi + E_{inv} + E_{vdW} + E_{Coul} \quad (1)$$

where E_l, E_θ, E_φ are the bond stretching, bond angle bending, and dihedral angle torsion, respectively, E_{inv} is the improper out-of-plane interaction, and E_{vdW} and E_{Coul} are the van der Waals and Coulombic interactions, respectively. The first four terms of Eq. (1) are bonded energies, and the last two terms of Eq. (1) are nonbonded energies. In calculating the nonbonded interactions, a cut-off distance of 9 Å was used along with a switching method. The spline switching method [50] was applied to smoothly reduce the interaction energies to zero by using the spline-on at 8.0 Å and the spline-off at 8.5 Å. All atoms in the mesogenic groups and in the backbone were assigned with partial charges calculated using the charge-equilibration algorithm [51] in Cerius^2. The criterion of energy convergence was to obtain a root mean square force less than 0.1 kcal mol^{-1} Å^{-1} in the simulated systems. Each cycle of energy minimization continued until convergence of the energy took place. In molecular dynamics runs, the time step, $\delta t = 1.0$ fs, was used to integrate the equations of motion for canonical dynamics by a leap frog Verlet algorithm [52]. The length of a molecular dynamics run was 20 ps. On each

model structure, 10–15 cycles of energy minimization and molecular dynamics were carried out. When the structures of the models became relaxed, further molecular dynamics runs were performed under an isothermal–isobaric (NPT) ensemble at a temperature of 373 K and a pressure of 1 atm in the duration of 300–500 ps to ensure that the systems approached equilibration in the smectic C phase. In the NPT ensemble, the canonical Nosé thermostat [45–47] was used to maintain a constant temperature, the Anderson–Parrinello–Rahman methods [53,54] were used to control the pressure and stress, and periodic boundary conditions [52] were applied to the models to conserve the number of atoms. Moreover, X-ray diffraction patterns were simulated on the basis of 10 equilibrated structures. Diffraction patterns for powders were simulated by using the Diffraction Crystal module in Cerius^2; the results were compared with the experimental results. All measurements for the smectic C phase were based on 10 equilibrated structures. Ten initial structures of an isolated PDMS chain with a repeat unit of 35 were relaxed and equilibrated in vacuum by similar procedures. These simulations were carried out on an IRIS Indigo^2 Impact 10,000 computer.

4. Results and discussion

4.1. Equilibration of the bulk systems

The equilibrated structures were obtained by performing further molecular dynamics runs under NPT conditions at a temperature of 373 K on the relaxed structures. Such a temperature was chosen according to experimental results, and this temperature fell within the temperature range for the S_{C*} phase of PS221B. Since a small deviation of the volume of a system may cause a tremendous variation in the potential energy, an easy way to monitor system equilibration was recording the instantaneous values of the potential energy during the equilibration period. Thus, the instantaneous values of the potential energy were recorded during a molecular dynamics run. Therefore, the fluctuations of quantities were observed during equilibration in systems. The equilibration period was determined by the amount of time it took for the dynamics of these quantities to fluctuate symmetrically with respect to their most probable values.

To determine the time required for the structures to gain their equilibration, initially, a molecular dynamics run (NPT) has been carried out for 500 ps on one of the 10 relaxed systems at 373 K. Fig. 6 shows the fluctuations of the potential energy of the system as a function of time. As Fig. 6 indicates, the total amount of time required for equilibration can be identified as 200 ps for the system. The averaged value of the potential energies was $-20{,}119.3 \pm 17.9$ kcal/mol. Following the equilibration run, molecular dynamics runs (NPT) were performed on the rest of the relaxed systems for 300 ps to equilibrate the systems. Fig. 7 displays one of the ten equilibrated structures. The averaged unit cell parameters and the averaged density for the equilibrated systems were obtained by averaging the 10 equilibrated structures. Table 1 shows the averaged cell parameters. The averaged density was 1.09 ± 0.01 g/cm^3,

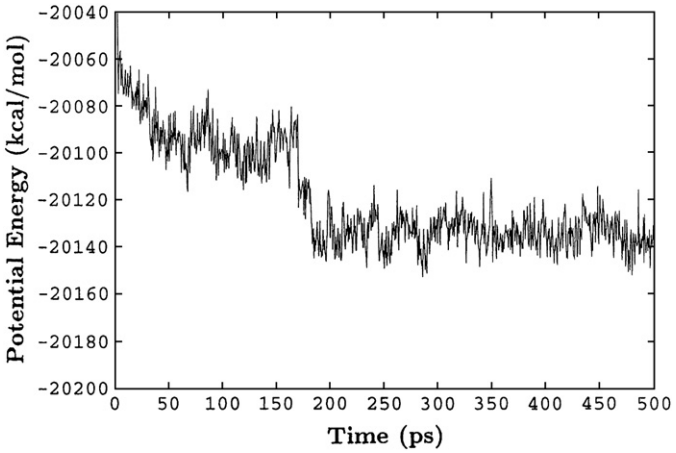

Fig. 6. Fluctuations of the potential energy obtained from a molecular dynamics run with simulation time for the system composed of a PS221B molecule at 373 K.

which is slightly lower than the experimental result, as shown in Section 2.

As shown in Fig. 7, this equilibrated structure is a unit cell with three-dimensional periodic boundaries, filled with a side-chain liquid crystalline polymer. The unit cell can be considered as one in three-dimensional space repeated infinitely.

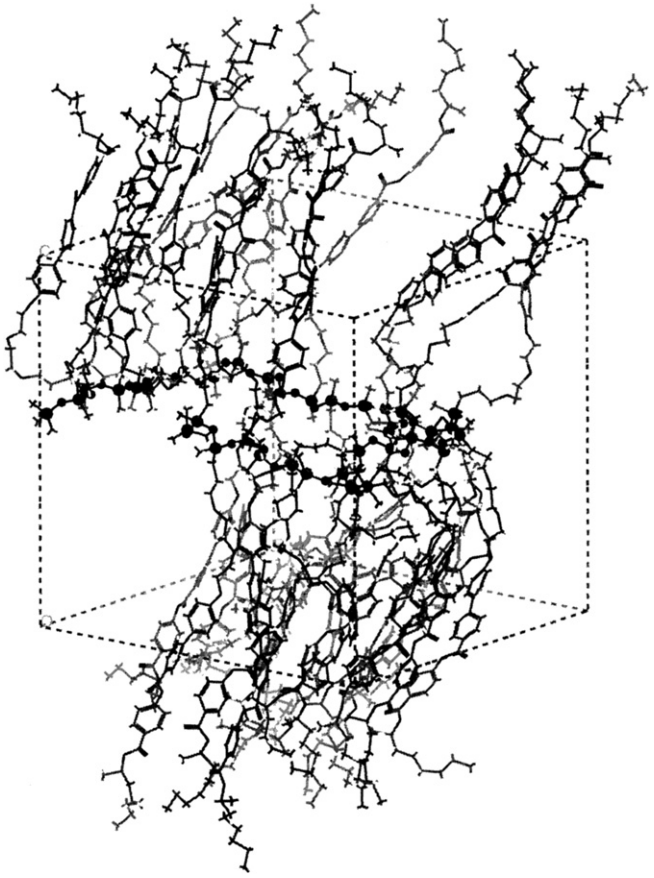

Fig. 7. An equilibrated structure shown with a periodic simulation cell to accommodate a PS221B molecule. The polysiloxane backbone is shown by a stick–ball representation.

Table 1
Unit cell parameters

I[a]		II[b]	
a	33.03 ± 0.16	*α*	90.20 ± 0.16
b	31.81 ± 0.08	*β*	90.18 ± 0.27
c	32.17 ± 0.11	*γ*	90.09 ± 0.24

[a] Unit cell dimensions (in Å).
[b] Unit cell angles (in degrees).

Fig. 8 shows a part of the entire assembly in which the primary cell (parent cell) is surrounded by 26 image cells. From the figure, it is clear that the side groups from the primary cell are completely interdigitated with those from the top or bottom image cells. As a consequence of this arrangement, it is readily apparent that the simulated models are generated by a monolayer smectic structure. Therefore, the *d*-spacing can be measured from the distance between the nearest two polysiloxane backbones.

Table 2 shows the internal stress tensor and the total potential energy for the 10 equilibrated structures. The components of the internal stress tensor were calculated by summing the forces acting on each pair of atoms in the system, formulated [42] as

$$\sigma_{ij} = \frac{\sum_{\mathrm{kl}} \left(r_i^{\mathrm{k}} - r_i^{\mathrm{l}}\right) f_j^{\mathrm{kl}}}{2V} \tag{2}$$

where r_i^{k} and r_i^{l} are the coordinates in the i direction for atom k and atom l, respectively, f_j^{kl} is the jth component of the force acting between the two atoms, and V is the volume of the system. As shown in Table 2, the values of the internal stress components among the 10 equilibrated structures are relatively small, although they are slightly higher than those found in the simulations of amorphous polymers [42–44]. The states for amorphous polymers have been relaxed and quenched at zero-temperature, whereas the systems prepared in our study were equilibrated at 373 K. Moreover, the positive and negative stresses indicate the expansion and compression, respectively, for unit cell dimensions. The last column in Table 2 lists the total potential energies, as obtained according to Eq. (1). The differences of the total potential energy among the 10 equilibrated structures are about 5%. The small differences

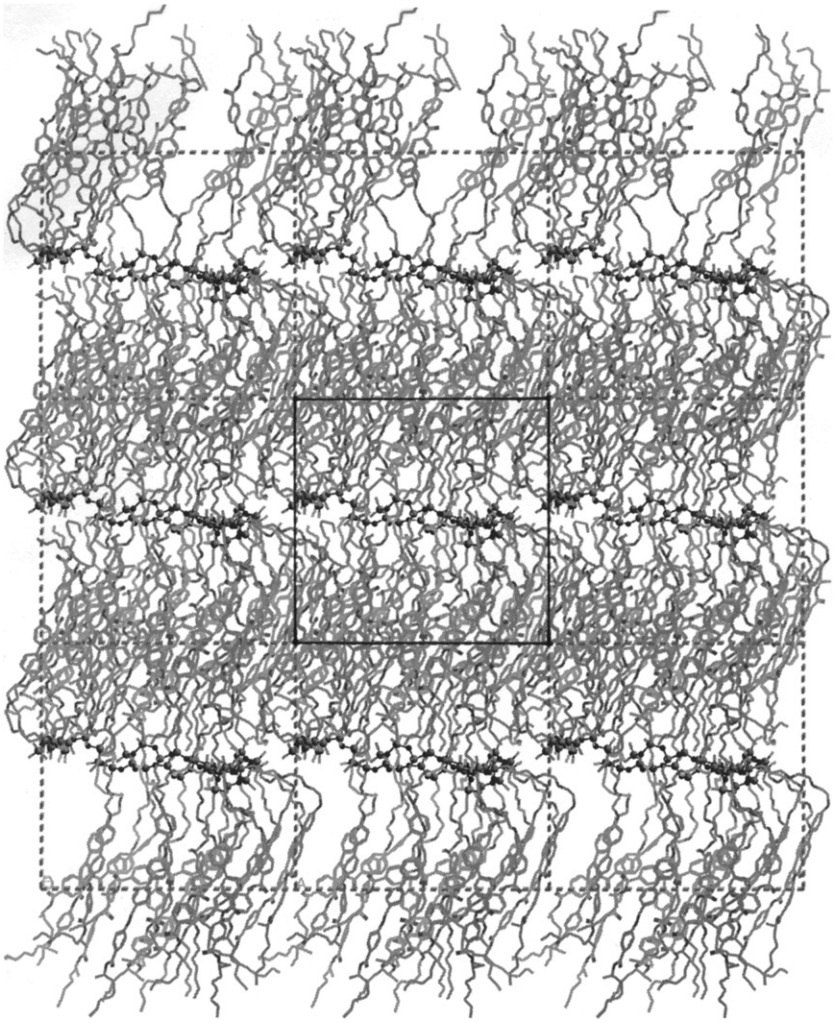

Fig. 8. A primary (parent) cell and eight of its neighboring images, projected on the *yz* plane. The primary cell, whose boundaries are drawn by heavy lines, is the same as that shown in Fig. 7; hydrogen atoms are omitted for clarity.

Table 2
Internal stress tensor (GPa) and total potential energy (kcal/mol)

I[a]	α_{xx}	α_{yy}	α_{zz}	α_{yz}	α_{xz}	α_{xy}	E_t (10^{-4})[b]
1	−0.241	0.208	−0.005	−0.347	−0.042	0.089	−2.015
2	0.098	−0.189	−0.008	−0.287	0.070	0.064	−2.036
3	−0.149	−0.163	0.017	−0.439	0.286	−0.218	−2.044
4	−0.138	0.143	0.046	−0.020	−0.361	−0.252	−1.939
5	0.022	0.102	−0.095	0.193	−0.206	−0.115	−1.998
6	−0.118	0.062	−0.032	0.348	0.055	−0.239	−1.951
7	−0.055	−0.318	0.226	0.188	0.173	0.083	−1.943
8	0.062	0.039	−0.262	−0.059	0.016	0.056	−1.994
9	0.071	−0.083	−0.034	−0.023	0.031	0.176	−1.950
10	0.252	−0.174	−0.116	0.140	−0.007	−0.061	−1.953

[a] Number of structures.
[b] Total potential energy in the equilibrated structures, as calculated according to Eq. (1).

between the total potential energies and the relatively small internal stresses indicate that these structures have obtained their equilibration [44].

4.2. Simulations of X-ray diffraction patterns

In order to show the corrections of the simulated systems, we have performed simulations of X-ray diffraction patterns on the already equilibrated structures. The simulated X-ray diffractions of the 10 equilibrated structures display very similar patterns to each other. For the structural comparison, the pairwise root mean square deviation (RMSD) was adopted. The pairwise RMSD was calculated for each pair of structures in the ensemble of the 10 equilibrated structures. The pairwise RMSD of structures a and b was calculated according to Eq. (3)

$$\mathrm{RMSD} = \left[\frac{1}{N}\sum_{i=1}^{N}\left(r_i^{\mathrm{a}} - r_i^{\mathrm{b}}\right)^2\right]^{1/2} \tag{3}$$

where r_i^{a} and r_i^{b} denote the Cartesian coordinate for atom i in structures a and b, respectively, and N is the number of atoms being monitored. The pairwise RMSD values among the 10 equilibrated structures were between 1.25 and 1.33 Å, indicating that these structures were close to each other.

Fig. 9 displays the simulation and experimental results of X-ray powder diffraction patterns. The solid line represents the resulting simulations of X-ray diffraction pattern (averaged), based on the 10 equilibrated structures. The broken line represents an experimental result, as obtained from the curve of 100 °C in Fig. 3. Comparing the simulated pattern with that from experiment indicates that the simulated pattern is in agreement with the one obtained experimentally. The simulated X-ray diffraction pattern depicted in Fig. 9 shows a sharp Bragg reflection at small angles corresponding to the smectic layers (d-spacings). The averaged value of the d-spacings can be evaluated as 32.13 ± 0.60 Å. In addition, a broad reflection at wide angles is associated with the lateral packing, which can be located at the position 2θ equal to $17.64 \pm 0.06°$, corresponding to 5.03 ± 0.02 Å. The averaged value of the d-spacings estimated by simulations is in good agreement with the experimental results. On the other hand, the averaged value of the lateral spacings obtained from the simulations is slightly higher than the experimental value (4.50 Å). Moreover, the broad reflection reveals that the order inside the smectic layers is liquid-like in the smectic liquid crystalline polymer.

4.3. Radius of gyration for the backbone

The configuration of the polysiloxane backbone confined between liquid crystal layers can be probed using its mean square radius of gyration $\langle R_{\mathrm{g}}^2 \rangle$, defined as follows [27]:

$$\left\langle R_{\mathrm{g}}^2 \right\rangle = \frac{1}{N_{\mathrm{a}}}\sum_{i=1}^{N_{\mathrm{a}}}\left(\mathbf{r}_i - \mathbf{r}_{\mathrm{CM}}\right)^2 \tag{4}$$

where N_{a} is the number of atoms in the backbone, and $\mathbf{r}_i$ is the position vector for the ith atom; $\mathbf{r}_{\mathrm{CM}}$ is the center of mass vector that is defined by

$$\mathbf{r}_{\mathrm{CM}} = \frac{1}{T_{\mathrm{Am}}}\sum_{i=1}^{N_{\mathrm{a}}}\mathbf{r}_i \mathrm{Am}_i \tag{5}$$

where Am_i is the atomic mass of the ith atom in the backbone, and T_{Am} is the total atomic mass. The results of the mean

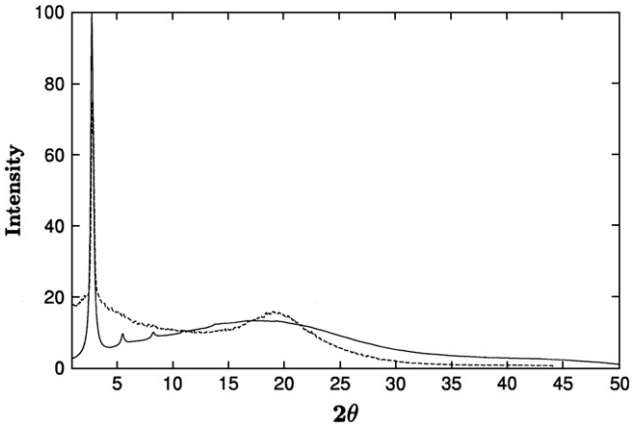

Fig. 9. Simulated (solid line) and experimental (broken line) X-ray diffraction patterns of PS221B in the smectic C phase. The solid line indicates the result estimated from the 10 equilibrated structures.

square radius of gyration for the backbone in the 10 equilibrated structures are entered in column 2 of Table 3. Data in column 3 of Table 3 represent the mean square radii of gyration in the z direction, $\langle R^2_{g,z}\rangle$. Values in column 2 are found to be about 20 fold higher than those listed in column 3. This finding suggests that the polysiloxane backbone is squeezed by the mesogenic groups along the z direction in the liquid crystalline state. If the values in column 3 are taken in a square root and then doubled; i.e., $2(\langle R^2_{g,z}\rangle)^{1/2}$, the resulting values correlate with the width of the backbone sublayers along the z direction. The values are listed in the last column of Table 3, and the average of these values is 5.63 ± 0.09 Å. Davidson et al. [25] have determined the width of polysiloxane backbones confined between liquid crystalline layers to be 5–7 Å by using X-ray diffraction methods. The averaged width of the backbone sublayers in the equilibrated structures falls within the experimental range.

4.4. Bond direction correlation function of the backbone

Another technique that may be also used to characterize the chain configuration of the polysiloxane backbone confined between liquid crystalline layers is the "bond direction correlation function", or "order parameter" [41,43]. The order parameter is defined as

$$S_{ij} = \frac{3\langle \cos^2\theta\rangle - 1}{2} \tag{6}$$

where θ is determined by the angle between any two skeletal bond chords, ij, for the backbone. Bond chord i is the vector drawn between the midpoint of the bond from atom $i-1$ to atom i, to the midpoint of the bond from atom i to atom $i+1$. The results, as calculated from the 10 equilibrated structures and from the 10 random configurations of an isolated PDMS chain, are shown as a function of index difference $|i-j|$ in Fig. 10 as a solid line and a broken line, respectively. The values of S_{ij} have been obtained from Eq. (6) by taking the average for the squared cosine of the angle between overall chord pairs along the backbone or the PDMS chain, and then averaged in the 10 structures. As shown in Fig. 10, there is a strong directional correlation when $|i-j|$ is less than 5, and this phenomenon can also be found in previous works [41,43]. If the configuration of a polymer chain is random, it will have a random distribution of skeletal chords; therefore, $\cos\theta$ becomes random, which leads to $S_{ij} = 0$, and thus the bond direction correlation function vanishes rapidly as the values of $|i-j|$ increase along the chain, as shown by the broken line in Fig. 10. However, as shown by the solid line in Fig. 10, the directional correlation function does not vanish when the values of $|i-j|$ become larger. The evidence that is not absent from long-range correlations may suggest that the configuration of the backbone, confined between liquid crystal layers in the equilibrated systems, is not as random as that of an isolated PDMS chain with the random structures.

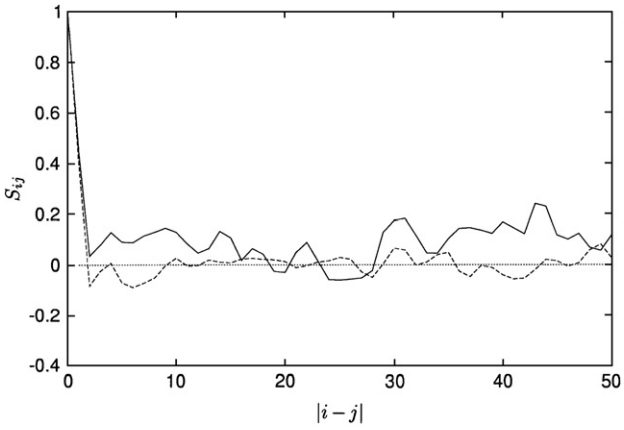

Fig. 10. Averaged bond direction correlation function S_{ij} for the polysiloxane backbone in the 10 equilibrated structures (solid line) and for the isolated PDMS chain with 10 random structures (broken line) versus the index difference $|i-j|$.

Table 3
Radius of gyration for the backbone

I[a]	$\langle R^2_g\rangle$[b]	$\langle R^2_{g,z}\rangle$[c]	D[d]
1	167.57	7.94	5.64
2	168.59	8.45	5.81
3	168.29	8.14	5.71
4	167.32	7.79	5.58
5	163.49	7.63	5.52
6	167.91	7.82	5.59
7	169.08	7.88	5.62
8	168.66	8.16	5.71
9	168.02	7.73	5.56
10	168.49	7.68	5.54

[a] Number of structures.
[b] Mean square radius of gyration (in Å^2).
[c] Mean square z-component of the radius of gyration (in Å^2).
[d] Values calculated using $2(\langle R^2_{g,z}\rangle)^{1/2}$ (in Å).

4.5. Distribution of the dihedral angles of the backbone

Fig. 11 depicts the probability distribution $P(\varphi_i)$ for the dihedral angles at the internal Si–O bonds, independent of the state of the neighbors. The solid line of Fig. 11 was obtained from the dihedral angles at the overall 700 Si–O bonds in the 10 equilibrated structures, and the broken line was obtained from those in the 10 random structures of an isolated PDMS chain. As shown in Fig. 11, it can be observed that the distributions of the dihedral angles fall in three different ranges centered at *trans* (180°), *gauche*$^+$ (60°), and *gauche*$^-$ (300°). By convention, the dihedral angle φ_i is therefore assigned to three rotational isomeric states. The *trans* (t) state is assigned for the range $120° < \varphi_i < 240°$, *gauche*$^+$ (g^+) for $0° < \varphi_i < 120°$, and *gauche*$^-$ (g^-) for $240° < \varphi_i < 360°$. The values of the probability for t, g^+, or g^- can be calculated directly from Fig. 11. The values associated with the polysiloxane backbone in the 10 equilibrated structures are 0.519, 0.245, and 0.236, and those corresponding to the isolated PDMS chain with the 10 random structures are 0.466, 0.229, 0.305 for the t, g^+, and g^-, respectively. As shown in Fig. 11, the isolated PDMS chain produces more preferred ranges of dihedral angles at t,

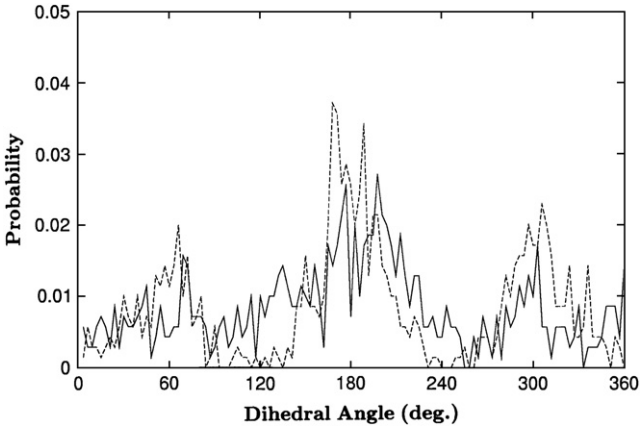

Fig. 11. Distributions of the dihedral angles at the internal Si–O bonds for the polysiloxane backbone in the 10 equilibrated structures (solid line) and for the isolated PDMS chain with 10 random structures (broken line), regardless of the state of the neighbors.

g^+, and g^- than the polysiloxane backbone does. On the other hand, the corresponding values of the probability, which have been obtained from molecular dynamics simulations at 300 K by Mattice et al. [55] on an isolated PDMS chain with the oligomer of eight units, gave 0.412, 0.289, and 0.289 for *t*, g^+, and g^-, respectively. The value for the *t* state, as obtained from the equilibrated structures, is higher than that obtained from the isolated PDMS chain with random structures and that from molecular dynamics simulations [55]. However, the equilibrated structures gave lower values for the *gauche* states. Such a high probability value for the *t* state may suggest that the configuration of the backbone is not as random as that of the isolated PDMS chain with random structures.

4.6. Distributions of consecutive dihedral angles of the backbone

The rotation of a bond in a polymer chain is related to the conformations of its neighboring bonds due to the steric repulsion of groups separated by the bonds [56]. Thus, the correlated distributions of dihedral angle pairs along the polymer chain are important. The consecutive dihedral angles (φ_i, φ_{i+1}) are defined by the pairs of bonds (O–Si, Si–O) and (Si–O, O–Si) in the polysiloxane backbone. Three stable rotational isomeric states are defined by the torsional angles of +180° (*t*), +60° (g^+), and +300° (g^-). Fig. 12a and b shows the distributions of dihedral angles, as calculated on the 10 equilibrated structures for the pairs centered on silicon and oxygen, respectively. The resulting distributions around the possible states (*t*, g^+, and g^-) are relatively broad and spread over a large area in the states. Since the distributions of the dihedral angles are spread over a large area around the states, it is hard to identify which state has a strong preference over the others. Although it is hard to find an exact location for each state, an approximate 3-fold conformation is still discernible. In Fig. 12a, the states *tt*, $tg^{\pm}$, and $g^{\pm}t$ can be found, but the states g^+g^- and g^-g^+ are completely suppressed. These states correspond to the results of local minimum energies calculated by

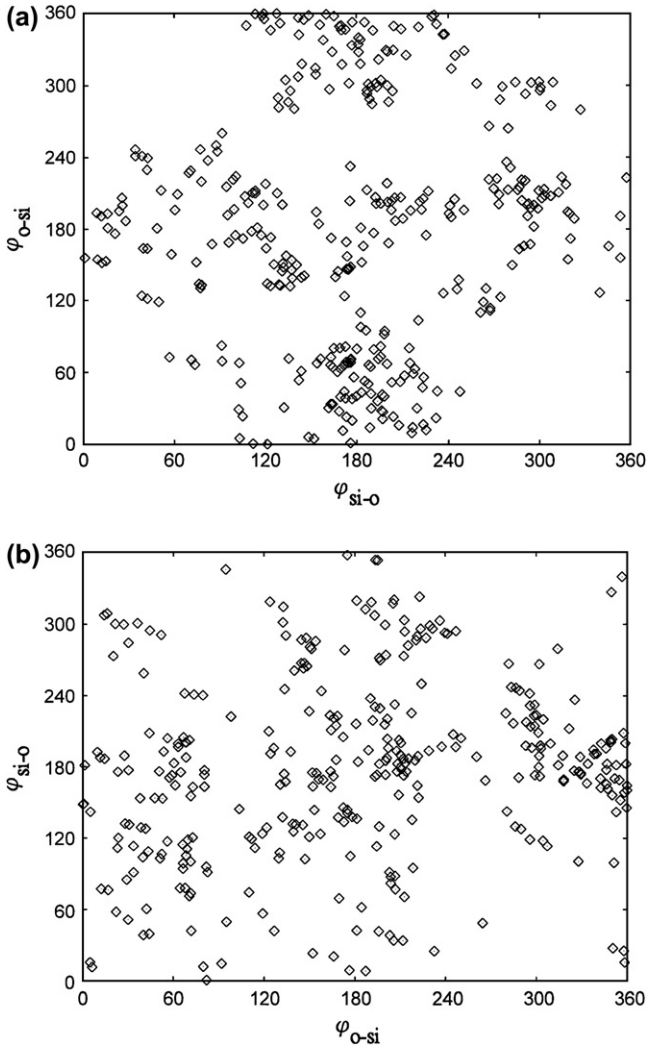

Fig. 12. Distribution of consecutive dihedral angles (φ_i, φ_{i+1}) for the polysiloxane backbone in the 10 equilibrated structures: (a) for the pair of bonds (O–Si, Si–O); (b) for the pair of bonds (Si–O, O–Si). The ordinate and the abscissa refer to the dihedral angles φ_i and φ_{i+1}, respectively.

Mattice et al. [55] using molecular mechanics calculations. On the contrary, points in the areas of $g^{\pm}g^{\pm}$ are relatively less frequent in Fig. 12a. As shown in Fig. 12b, the distributions of the dihedral angles are spread out, making it harder to identify the stable states. However, the distributions around the states such as *tt*, $tg^{\pm}$, and $g^{\pm}t$ can be found. On the other hand, points around the states such as $g^{\pm}g^{\mp}$ and $g^{\pm}g^{\pm}$ appear less frequent than the corresponding states calculated by Mattice et al. To facilitate a comparison, Fig. 13a and b displays the distributions of the dihedral angles, as calculated on the 10 random structures of an isolated PDMS chain, for the same pairs of bonds as shown in Fig. 12a and b. It is clear that Fig. 13a and b displays much denser distributions. Therefore, the most probable states, such as *t*, g^+, and g^- can be easily identified. As shown in Fig. 13a, the points around the $tg^{\pm}$ and $g^{\pm}t$ states are more frequent than those around the *tt* state, giving a result that corresponds to the works of Mattice et al. [55]. Furthermore, the *tt* state in Fig. 12a is more probable than

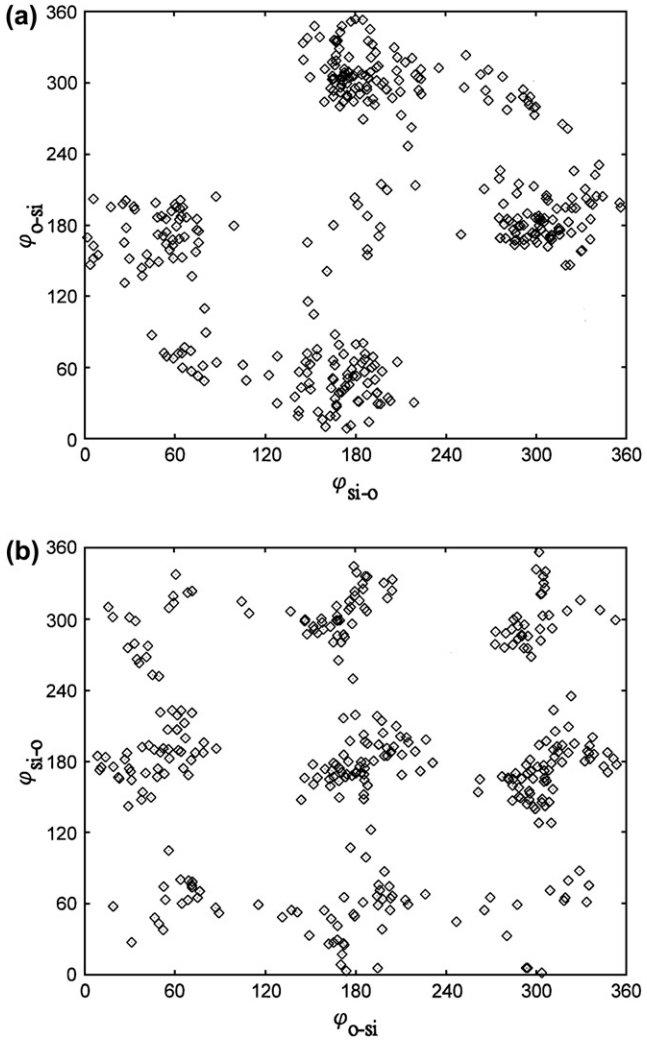

Fig. 13. Distribution of consecutive dihedral angles (φ_i, φ_{i+1}) for an isolated PDMS chain with a repeat unit of 35, generated with 10 random structures: (a) for the pair of bonds (O–Si, Si–O); (b) for the pair of bonds (Si–O, O–Si). The ordinate and the abscissa refer to the dihedral angles φ_i and φ_{i+1}, respectively.

the same state in Fig. 13a. This may support the fact that the polysiloxane backbone is constrained by liquid crystal layers, thereby causing the backbone to lose its randomization.

4.7. Distributions of the dihedral angles of the aromatic core in the mesogens

Fig. 14 shows the distributions of the dihedral angles at bonds ϕ_1, ϕ_2, ϕ_3, ϕ_4, and ϕ_5 in the aromatic core of the mesogenic groups. The indices for the bonds ϕ_1 through ϕ_5 correspond to those indexed as 1–5 in Fig. 1. In the calculations, the distributions of dihedral angles were evaluated according to the 10 equilibrated structures. The range of dihedral angle, ϕ, is reported as 0–360°. Thus, the *cis* placement is centered at 0° or 360°, and the *trans* placement is around 180°. Fig. 14 clearly reveals that the most probable values of the distributions of the dihedral angles can be classified into two regions: one is around the *cis* conformation, such as ϕ_1 and ϕ_4, and the

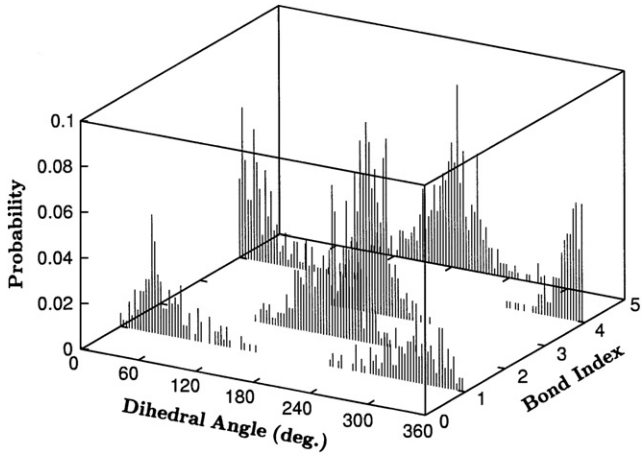

Fig. 14. Distributions of the dihedral angles at the internal C–C or C–O bonds of the aromatic core in the mesogenic groups in the 10 equilibrated structures. The bonds indexed by 1 (ϕ_1) through 5 (ϕ_5) correspond to the indices shown in Fig. 1.

other is centered at the *trans* conformation, such as ϕ_2, ϕ_3, and ϕ_5. Furthermore, the dihedral angles at the bonds in the aromatic core fluctuate about their most probable values, and the magnitude, $\delta\phi$, of the fluctuations of a dihedral angle is formulated as

$$\delta\phi = \left(\langle\phi^2\rangle - \langle\phi\rangle^2\right)^{1/2}, \tag{7}$$

where the angular brackets denote the statistical averages of the enclosed quantity. A mean value in $\langle\phi\rangle$ denotes the precise location of the most probable appearance of a dihedral angle, and a value of $\delta\phi$ represents the breadth of fluctuations for a dihedral angle. The distribution curve for ϕ_1 in Fig. 14 is split into two regions. The calculations of $\langle\phi\rangle$ and $\delta\phi$ are dependent on the two regions, and the values of $\langle\phi\rangle$ and $\delta\phi$ are 48.5 ± 26.7 for the positive region and $309.6\ (-50.4) \pm 26.7$ for the negative region. The other values are 179.9 ± 29.1, 180.4 ± 17.0, 6.5 ± 30.1, and 183.5 ± 32.0 for ϕ_2 through ϕ_5, respectively. Using single-crystal X-ray analysis for the compounds containing the biphenyl group, the values of the dihedral angle between the two benzene rings of the biphenyl group have been determined to fall between ±37° and ±65° [57–59]. In our previous work [16], the AM1 calculations of the biphenyl group in the aromatic core for the isolated monomers also indicated that the values of the dihedral angle are ±40. Thus, the most probable values found for ϕ_1 reasonably fall within this range. On the other hand, the values of $\langle\phi_4\rangle$ are smaller than those obtained by experimental results, which have been found in the range between ±55° and ±57° [60,61]. The most probable values for ϕ_2, ϕ_3, and ϕ_5 correspond well with those found in previous investigations [16,35,36,62]. As shown in the above values, the distribution of the dihedral angle at ϕ_3 has the smallest value of $\delta\phi$ because the C–O bond (ϕ_3) of the ester group has a significant double bond character due to resonance with the carbonyl group. Therefore, the most probable appearance of the *cis* and *trans* placements suggests that the Ph–Ph–COO–Ph

fragment in the mesogens is favorable for the interactions between mesogenic groups at the aromatic cores.

4.8. Orientation of the mesogens

A technique that can be used to study the orientation of the mesogens is the averaged second-order Legendre polynomial, which has been called the order parameter. In the simulations, the definition of the order parameter $S(\mathbf{n})$ is the same as that in Eq. (6); i.e., S_{ij} is replaced by $S(\mathbf{n})$, where $\mathbf{n}$ is the liquid crystalline director, obtained from the average of the direction vectors of the mesogens in a simulated system. The direction vector for each mesogen is taken from the first carbon in the core part to the last one of the same part, and θ in Eq. (6) is replaced by $\theta_{i,\mathbf{n}}$, which is the angle between $\mathbf{n}$ and the direction vector of each mesogen i. $S(\mathbf{n})$ implies the following conditions: (a) if the mesogens are completely parallel to the director $\mathbf{n}$, then $S(\mathbf{n}) = 1$; (b) if the mesogens are in random orientations, then $S(\mathbf{n}) = 0$; and (c) if the mesogens are normal to the director $\mathbf{n}$, then $S(\mathbf{n}) = -0.5$. The cases (a) and (c) are the two extreme limits. The order parameters are calculated for the upper mesogens and for the lower ones, respectively. The definition of the upper or lower mesogens is based on the location of mesogens above or below the backbone, as shown in Fig. 7. The averaged order parameters, as calculated on the 10 equilibrated structures, are 0.91 ± 0.08 and 0.86 ± 0.15 for mesogens in the upward direction and for those in the downward direction, respectively. These values slightly deviate from unity, indicating that the mesogens in the simulated systems have a high level of order. This may be due to the fact that the interactions between mesogens are favorable, as mentioned in Section 4.7.

As shown in Fig. 3, the d-spacings decrease as the measuring temperature decreases, due to the fact that the tilt angle for PS221B increases as the measuring temperature decreases. The orientation of the mesogens may also be represented by the tilt angle, calculated as

$$\theta = \cos^{-1}(d_C/d_l), \tag{8}$$

where d_C is the averaged value of the simulated d-spacings in the smectic C phase, and d_l is the averaged length of the mesogenic groups in the simulated cells. The averaged value of the tilt angle, based on the 10 equilibrated structures, is $12.01 \pm 0.76^\circ$, which corresponds to those evaluated for the similar compound, PS212A [8], on the basis of X-ray diffraction patterns.

4.9. Radial distribution functions

The local structure of a simulated system can be described by the radial distribution functions, which reveal the correlations of a specific pair of atom types. The radial distribution function, $g_{AB}(r)$, is calculated as the statistical relationship of a given atom A, positioned at a certain point in a simulated system, with the number of B atoms in a spherical cell of radius r and thickness Δr about atom A. The relation is formulated as follows [52]:

$$g_{AB}(r) = \frac{\langle N_{AB}(r)\rangle}{4\pi r^2 \Delta r \rho}, \tag{9}$$

where $\langle N_{AB}(r)\rangle$ is the averaged number of AB pairs in a spherical shell located between r and Δr and ρ is the bulk density. In the results, $\Delta r = 0.03$ Å has been used. The radial distribution functions have been used to investigate a detailed molecular structure for amorphous polymers [41–44]. The radial distribution functions have also been reported in the literature [33,37,63–65] of liquid crystalline systems using computer simulations.

For the equilibrated structures, there are three distinct atom pairs in the mesogenic groups: the carbon–carbon, the carbon–hydrogen, and the carbon–oxygen. Fig. 15a–c depicts the radial distribution functions for the atom pairs, the C, C, the C, H, and the C, O, respectively, as calculated by averaging the 10 equilibrated structures as a function of the distance r. The figures clearly indicate that similar radial distribution functions were obtained for the three pairs of atoms; i.e., the radial distribution functions exhibit no sign of order when the distance r is greater than 5 Å.

As shown in Fig. 15, the peaks that appear due to intramolecular connections can be observed when the distance r is less than 3 Å. The sharp peaks correspond to the distances, which can be assigned by the length of chemical bonds or derived from a pair of bonds. These distances do not depend on the conformations of the mesogenic groups, so they gave rise to the sharp peaks in the radial distribution functions. As mentioned in the above section, due to lateral packing, the most probable value of the aromatic core overlap between the mesogens was $\sim$5.03 Å, indicating that there is a local order in this range between aromatic cores. Beyond this distance, the structures of the simulated systems become random because distances between two neighboring atoms are not as fixed as those in the local order. As a result, there is no sign of order in these figures when the distance r is greater than 5 Å.

5. Conclusions

The compound PS221B has been investigated using atom-based molecular modeling. Simulations have been conducted with the aid of Cerius^2. For simulations, 10 starting models with periodic boxes have been generated using molecular dynamics. The models achieved relaxation by combining energy minimizations and molecular dynamics runs under a canonical (NVT) ensemble, and approached equilibrated states by conducting further molecular dynamics runs under an isothermal–isobaric (NPT) ensemble. These equilibrated structures have been verified by simulated X-ray diffraction patterns, which are in satisfactory agreement with those obtained experimentally. For the polysiloxane backbone in the equilibrated structures, the bond direction correlation function does not vanish its correlations of long-range order, and also a high probability value of the distribution of the dihedral angles

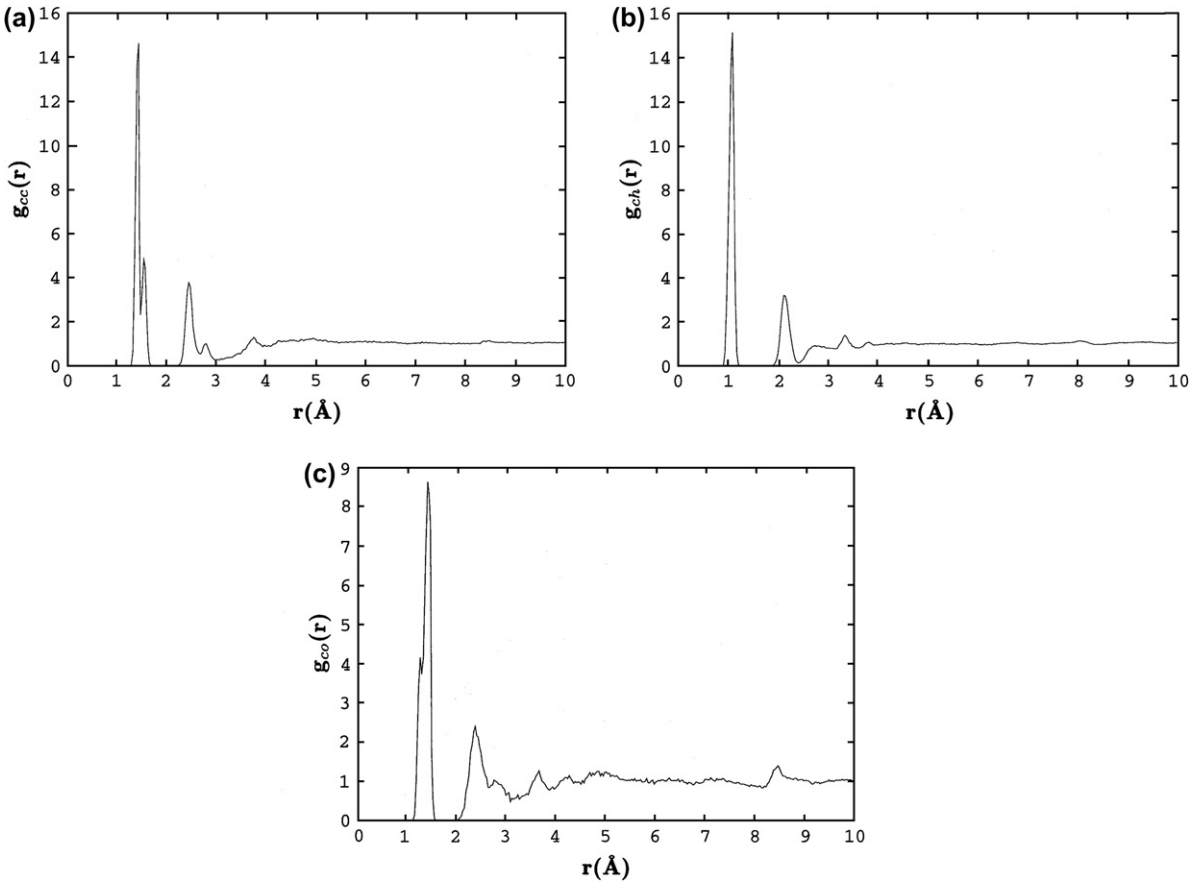

Fig. 15. Radial distribution functions of the 10 equilibrated structures for (a) carbon–carbon, (b) carbon–hydrogen, and (c) carbon–oxygen.

can be found in the *trans* state. These findings may suggest that the configuration of the polysiloxane backbone is not as random as that of an isolated PDMS chain with random structures. The width of the backbone sublayers with an averaged value of 5.63 ± 0.09 Å falls within the range of experimental results [25]. This suggests that the backbone confined between liquid crystal layers has a configuration which is squeezed in the z direction to a quasi-bidimensional random coil. The consecutive bonds in the polysiloxane backbone in the equilibrated structures produce a wide-spread distribution of rotational isomeric states, which are hard to distinguish between the states. On the other hand, the bond pairs investigated using the random configurations of an isolated PDMS chain produce the rotational isomeric states, which can be more easily identified when compared to those found in the backbone. For the mesogenic groups, their orientational behavior has been characterized by a tilt angle and by the order parameters, which show a high level of order in the equilibrated structures. The distributions of the dihedral angles at the bonds in the aromatic core of the mesogenic groups indicate that there are two regions for the most probable appearance of the distributions. The distributions for ϕ_1 and ϕ_4 are around the *cis* placement, and those for ϕ_2, ϕ_3, and ϕ_5 are centered at the *trans* placement. These placements favor the interactions between mesogenic groups, probably supporting the fact that high values of the order parameters can be found in the equilibrated systems. Also, the high order of arrangements in the mesogenic groups may cause a local order. The lateral packing found in the simulated X-ray diffraction pattern has indicated that the most probable value of the range of aromatic core overlap is $\sim$5.03 Å. The radial distribution functions, as calculated for the carbon–carbon, the carbon–hydrogen, and the carbon–oxygen, have a similar appearance; i.e., no visible peaks appear when the distance r is greater than 5 Å. The results may suggest that, in the equilibrated structures, there is a local order in the range of 3–5 Å between the aromatic fragments due to the van der Waals interactions.

Acknowledgments

The authors would like to thank the National Science Council of the Republic of China for financial support of this work under Contract No. NSC-87-2216-E007-032. The National Center for High-Performance Computing in Taiwan is gratefully acknowledged for providing computer facilities. Ms. Chuan-Mei Lee of Stanford University has helped with English editing of this manuscript.

References

[1] Gray GW, Goodby JW. Smectic liquid crystals: textures and structures. Glasgow: Leonard-Hill; 1984.

[2] Collyer AA, editor. Liquid crystal polymers: from structures to applications. London: Elsevier Applied Science; 1992.
[3] Blinov LM, Chigrinov VG. Electrooptic effects in liquid crystal materials. New York: Springer-Verlag; 1994.
[4] Chen J-H, Chang R-C, Hsiue G-H, Guu F-W, Wu S-L. Liq Cryst 1995;18:291–301.
[5] Hsiue G-H, Hwang C-P, Chen J-H, Chang R-C. Liq Cryst 1996;20: 45–57.
[6] Hsiue G-H, Wu J-L, Chen J-H. Liq Cryst 1996;21:449–59.
[7] Hsu C-S, Shih L-J, Hsiue G-H. Macromolecules 1993;26:3161–7.
[8] Hsiue G-H, Chen J-H. Macromolecules 1995;28:4366–76.
[9] Chen J-H, Hsiue G-H, Hwang C-P. Chem Mater 1997;9:51–60.
[10] Sha Y-A, Hsiue G-H, Chiu C-H, Jeng R-J, Tai H-C. Liq Cryst 2003;30:71–80.
[11] Keller EN, Halfon R, Nachaliel E, Davidov D, Zimmermann H. Phys Rev Lett 1988;61:1206–9.
[12] Yamaguchi T, Asada T. Liq Cryst 1991;10:215–28.
[13] Dunmur DA, Wilson MR. Mol Simul 1989;4:37–59.
[14] Keller EN. Macromolecules 1989;22:4597–9.
[15] Patnaik SS, Lupo JA, Pachter R. Comput Theor Polym Sci 1998;8: 39–47.
[16] Lee K-J, Hsiue G-H, Wu J-L, Chen J-H. Liq Cryst 1998;25:661–78.
[17] Mercurieva A, Birshtein T. Macromol Theory Simul 1995;4:629–41.
[18] Madhusudana NV, Rajan J. Liq Cryst 1990;7:31–40.
[19] Govind AS, Madhusudana NV. Liq Cryst 1993;14:1539–51.
[20] Lee K-J, Hsiue G-H, Wu J-L, Chen J-H. Liq Cryst 1999;26:469–82.
[21] Noirez L, Cotton JP, Hardouin F, Keller P, Moussa F, Pépy G, et al. Macromolecules 1988;21:2889–91.
[22] Noirez L, Keller P, Cotton JP. Liq Cryst 1995;18:129–48.
[23] Lecommandoux S, Noirez L, Achard MF, Hardouin F. J Phys II (France) 1997;7:1417–24.
[24] Rousseau D, Marty JD, Mauzac M, Martinoty P, Brandt A, Guenet JM. Polymer 2003;44:2049–55.
[25] Davidson P, Levelut AM, Achard MF, Hardouin F. Liq Cryst 1989;4:561–71.
[26] Davidson P, Levelut AM. Liq Cryst 1992;11:469–517.
[27] Kumar SK, Vacatello M, Yoon DY. J Chem Phys 1988;89:5206–15.
[28] Bitsanis I, Hadziioannou G. J Chem Phys 1990;92:3827–47.
[29] Cifra P, Bleha T. Macromol Theory Simul 2000;9:555–63.
[30] For reviews, see:
(a) Ilnytskyi JM, Wilson MR. J Mol Liq 2001;92:21–8;
(b) Bates MA. Liq Cryst 2005;32:1365–77;
(c) Wilson MR. Int Rev Phys Chem 2005;24:421–55.
[31] Podojil GM, Farmer BL, Adams WW. Polymer 1996;37:1825–32.
[32] Patnaik SS, Plimpton SJ, Pachter R, Adams WW. Liq Cryst 1995;19:213–20.
[33] Stimson LM, Wilson MR. J Chem Phys 2005;123:34908–17.
[34] Ilnytskyi J, Saphiannikova M, Neher D. Condens Matter Phys 2006;9:87–94.
[35] Hofmann D, Schneider AI, Blackwell J. Polymer 1994;35:5603–10.
[36] Ishaq M, Blackwell J, Chvalun SN. Polymer 1996;37:1765–74.
[37] Lyulin AV, Al-Barwani MS, Allen MP, Wilson MR, Neelov I, Allsopp NK. Macromolecules 1998;31:4626–34.
[38] Bharadwaj RK, Boyd RH. Macromolecules 1998;31:7682–90.
[39] Yung KL, He L, Xu Y, Shen YW. Polymer 2006;47:4454–60.
[40] Wu J-L. MS thesis. National Tsing Hua University; 1996.
[41] Theodorou DN, Suter UW. Macromolecules 1985;18:1467–78.
[42] Fan CF, Hsu SL. Macromolecules 1991;24:6244–9.
[43] Lee K-J, Mattice WL. Comput Polym Sci 1992;2:55–63.
[44] Li Y, Mattice WL. Macromolecules 1992;25:4942–7.
[45] Nosé S. J Chem Phys 1984;81:511–9.
[46] Nosé S. Mol Phys 1984;52:255–68.
[47] Nosé S. Prog Theor Phys Suppl 1991;103:1–46.
[48] Mayo SL, Olafson BD, Goddard WA. J Phys Chem 1990;94:8897–909.
[49] Accelrys, Inc., San Diego, CA, USA.
[50] Cerius^2 4.5 Forcefield-based simulations.
[51] Rappé AK, Goddard WA. J Phys Chem 1991;95:3358–63.
[52] Allen MP, Tildesley DJ. Computer simulation of liquids. Oxford: Clarendon Press; 1987.
[53] Andersen HC. J Chem Phys 1980;72:2384–93.
[54] Parrinello M, Rahman A. J Appl Phys 1981;52:7182–90.
[55] Bahar I, Zuniga I, Dodge R, Mattice WL. Macromolecules 1991;24:2986–92.
[56] Flory PJ. Statistical mechanics of chain molecules. New York: Interscience; 1969.
[57] Hori K, Ohashi Y. Bull Chem Soc Jpn 1988;61:3859–67.
[58] Ito K, Endo K, Hori K, Nemoto T, Uekusa H, Ohashi Y. Liq Cryst 1994;17:747–58.
[59] Kitano Y, Usami I, Obata Y, Okuyama K, Jinda T. Polymer 1995; 36:1123–6.
[60] Adams JM, Morsi SE. Acta Crystallogr 1976;B32:1345–7.
[61] Kaiser J, Richter R, Lemke G, Golič L. Acta Crystallogr 1980;B36: 193–5.
[62] Aoto M, Okazaki K. Ferroelectrics 1993;148:51–7.
[63] Aoki KM, Yonezawa F. Liq Cryst 1993;14:1237–42.
[64] Wilson MR, Allen MP. Mol Phys 1993;80:277–95.
[65] La Penna G, Catalano D, Veracini CA. J Chem Phys 1996;105:7097–110.